Published in final edited form as:
Biochim Biophys Acta. 2014 January ; 1840(1): 656–666. doi:10.1016/j.bbagen.2013.10.028.

Palmitate Interaction with Physiological States of Myoglobin

Lifan Shih, **Youngran Chung**, **Renuka Sriram**, and **Thomas Jue**
Biochemistry and Molecular Medicine, University of California Davis, Davis, CA 95616

Abstract

Background—Previous studies have shown that palmitate (PA) can bind specifically and non-specifically to Fe (III) MbCN. The present study has observed PA interaction with physiological states of Fe (II) Mb, and the observations support the hypothesis that Mb may have a potential role in facilitating intracellular fatty acid transport.

Methods—^{1}H NMR spectra measurements of the Mb signal during PA titration show signal changes consistent with specific and non-specific binding.

Results—Palmitate (PA) interacts differently with physiological states of Mb. Deoxy Mb does not interact specifically or non-specifically with PA, while the carbonmonoxy myoglobin (MbCO) interaction with PA decreases the intensity of selective signals and produces a 0.15 ppm upfield shift of the PA methylene peak. The selective signal change upon PA titration provides a basis to determine an apparent PA binding constant, which serves to create a model comparing the competitive PA binding and facilitated fatty acid transport of Mb and fatty acid binding protein (FABP).

Conclusions—Given contrasting PA interaction of ligated vs. unligated Mb, the cellular fatty acid binding protein (FABP) and Mb concentration in the cell, the reported cellular diffusion coefficients, the PA dissociation constants from ligated Mb and FABP, a fatty acid flux model suggests that Mb can compete with FABP transporting cellular fatty acid.

General Significance—Under oxygenated conditions and continuous energy demand, Mb, dependent fatty acid transport could influence the cell's preference for carbohydrate or fatty acid as a fuel source and regulate fatty acid metabolism.

Keywords

Lipid; fatty acid; NMR; metabolism; bioenergetics

1. INTRODUCTION

Biochemistry textbooks have codified the function of Mb as an O_2 store or O_2 facilitated transporter. Yet, after half a century of research, questions still remain about Mb structure and function [29,72,73]. Certainly, experiments have demonstrated the importance of Mb in supplying O_2 in plants and in mammalian tissue. Indeed, *in vivo* NMR experiments have observed Mb releasing its O_2 store to sustain oxidative metabolism during apnea in seals and

Correspondence: Dr. Thomas Jue, Biochemistry and Molecular Medicine, University of California Davis, Davis, CA 95616-8635, Phone: (530) 752-4569, FAX: (530) 752-3516, TJue@ucdavis.edu.

at the initiation of skeletal muscle contraction [11,52]. Yet the O_2 store of Mb can prolong respiration in a rat heart for only a few seconds during anoxia [10]. Upon CO inactivation of Mb function, the myocardium shows no compensating alteration in bioenergetics or contractile function response [9,20]. A mouse without Mb exhibits no striking impairments in its oxygen consumption rate, contractile function, bioenergetics, and metabolism [19,27]. Some researchers have now imputed a controversial NO bioscavenging and reductase function to Mb [18,35,37,57].

In the mouse model without Mb, myocardial metabolism switches its substrate preference from fatty acid to glucose. Fatty acid to glucose utilization ratio drops from 3/1 to 0.7/1 [17]. Given the conventional line of reasoning, the decline in oxidative fatty acid metabolism arises from a deficiency in Mb facilitated O_2 transport [17]. However, Mb appears to diffuse too slowly to compete effectively with free O_2 in normoxic heart [42,43,50,51]. Alternatively, the absence of Mb might indicate a diminished capacity to facilitate fatty acid transport. Indeed, early studies have suggested that Mb can bind fatty acid [25,26,28].

^{1}H NMR studies have recently interrogated the interaction of palmitate (PA) with Fe (III) MbCN and have found evidence for specific and non-specific binding [67]. Many studies use the paramagnetic Fe (III) MbCN as a structure-function model of the ligated physiological state of Mb, as represented by the diamagnetic Fe (II) MbO_2 or MbCO found in the cell, because the electron-nuclear interaction of the unpaired Fe(III) electron hyperfine shifts the heme and localized heme pocket amino acid residue signals into observable parts of the NMR spectral window [16]. The observation implies that PA also interacts with the physiological states of Mb.

Indeed, PA does interact specifically and non-specifically with MbCO, consistent with its interaction with MbCN. MbCO also increases PA solubility. However, PA does not appear to interact with deoxy Mb. The results suggest that ligated and unligated states of Mb exhibit distinct interactions with fatty acid and give rise to a modified view of intracellular fatty acid transport. Given the cellular Mb and fatty acid binding protein (FABP) diffusion coefficients, concentrations, and PA binding affinities, a fatty acid flux model indicates that ligated Mb can compete effectively with FABP to facilitate fatty acid transport [23,42,43]. Since deoxy Mb does not appear to interact with fatty acid, the differential interaction of ligated and unligated Mb suggests a convenient mechanism for fatty acid to load at the sarcolemma in the vicinity of a high PO_2 and unload the fatty acid and oxygen at the mitochondria in the environment of low PO_2. Mb can then follow the intracellular O_2 gradient from sarcolemma to the mitochondria to load and unload both fatty acid and oxygen without a need to invoke a complex explanation or mechanism as in the case with the high affinity FABP [71].

2. MATERIALS AND METHODS

2.1 Protein Preparation

Myoglobin and albumin solutions were prepared from lyophilized horse heart protein and essentially fatty acid free bovine serum albumin (Sigma Chemical Inc., St. Louis, MO). DeoxyMb was prepared from lyophilized metMb as described previously [36]. The preparation of MbCO solution followed a similar procedure. Dissolved oxygen from the metMb was removed and replaced with N_2. A 5 time excess of sodium dithionite was then injected to reduce the Fe (III) metMb to Fe(II) deoxy Mb and to remove any residual O_2. In the preparation of MbCO, the metMb solution was equilibrated with CO. The resultant MbCO solution was loaded on a Sephadex G-25 column equilibrated with 30mM Tris and 1mM EDTA at pH 7.4. Elution with the same buffer removed the dithionite from the

MbCO. Additional CO was then bubbled into the final MbCO solution. NMR tubes were sealed tightly with a rubber stopper.

Throughout the procedure, the pH was maintained

2.2 Fatty Acid-Mb Preparation

Sodium palmitate (Sigma Chemical Inc., St. Louis, MO) was dissolved in 30mM Tris buffer with 1mM EDTA at pH 8.5 at 65°C. Stock solutions of 10mM and 100mM were prepared and kept in a heating block (Thermolyne 17600 Dri-Bath) at 65°C. An aliquot of 10mM or 100 mM PA in Tris buffer at 65°C was added to 600ul of 0.2–0.8 mM myoglobin at 35°C to yield a final solution with Mb:PA ratios from 1:0.1 to 1:4. All NMR experiments were then conducted at 35°C. The time between PA addition and the start of the NMR measurement was approximately 5 minutes. The pH was measured at 35°C using a calomel electrode (Orion 7110BN Micro Calomel pH, Thermo Electron Corporation).

2.3 NMR

Bruker Avance 500 and 600 MHz spectrometers measured the ^{1}H signals with a 5 mm probe. The ^{1}H 90o pulse, calibrated against the D_2O signal from a 0.15 M NaCl solution, was 9 μs. Watergate pulse sequence was used to obtain solvent suppression. Sodium-3-(trimethylsilyl) propionate 2,2,3,3 d4 (TSP) served as the internal chemical shift and concentration reference. All samples contained 5% D_2O to enable the deuterium lock during signal acquisition. All measurements were carried out at 35°C. A typical spectrum required 1024 scans and used the following signal acquisition parameters: 12 KHz spectral width, 2,560 data points, and 107ms recycle time. Zero-filling the free induction decay (FID) and apodizing with an exponential window function improved the spectra. A spline fit then smoothed the baseline.

The ^{13}C signals collected at 151 MHz used the following acquisition parameters: 8.25 μs 90 pulse, a 33 KHz spectral window, and 16K data point. A GARP pulse sequence decoupled the ^{1}H signals, and $^{13}C_2$ acetate provided an internal chemical shift reference at 24.2 ppm.

2.4 Intracellular Fatty Acid transport

The intracellular fatty acid flux has contributions from free PA diffusion and protein mediated PA diffusion as expressed in the following equation, which approximates a zero free PA at the mitochondrial surface:

$$J = D_{PA} PA + D_X C_X \frac{PA}{K_D^X + PA} \quad (1)$$

J=the overall fatty acid flux, PA=soluble concentration of PA; C_X = cellular concentration of Mb or FABP; D_{PA}=diffusion coefficient of free PA, D_X = diffusion coefficient of Mb or FABP in the cell, $K_D^X = in\ vitro$ PA dissociation constant of Mb or FABP [42,43,45,59,67]. Because the reported D_{PA} in the cell varies widely from 3.5×10^{-9} cm^2s^{-1} to 4.6×10^{-6} cm^2s^{-1}, the model has used the highest value to set an upper bound for free acid contribution [45,68]. The model also assumes an identical *in vitro* and *in vivo* K_D^X.

2.5 Statistical Analysis

Statistical analysis used the Sigma Plot/ Sigma Stat program (Systat Software, Inc., Point Richmond, CA) and expressed the data as mean value ± standard error (SE). Nonlinear regression analysis of the average data points determined the dissociation constant using

Marquardt-Levenberg algorithm. Statistical significance was determined by Student's t-test, $P<0.05$.

3. RESULTS

PA does not appear to interact with Fe (II) deoxy Mb. In the presence of PA, the hyperfine-shifted resonances of deoxy Mb exhibit no significant change in signal intensity or chemical shift, fig 1.

Moreover, no PA signal appears in the diamagnetic region of the deoxy Mb spectra, where the dominant PA $–CH_2$ signal would resonate, fig 2. Fig 2A shows the control spectrum of 0.8mM deoxy Mb in 30mM Tris buffer with 1mM EDTA at pH of 7.4 at 35°C. The addition of PA does not produce any detectable PA $–CH_2$ signal, fig 2B–2C. Dithionite, a chemical required to produce deoxy Mb, does not alter either the PA $–CH_2$ signal intensity or chemical shift (data not shown).

In contrast, PA interacts specifically with MbCO. Fig 3 shows the MbCO spectra response during a PA titration. The peaks (u3, u4, u5, u7, and u8) in the spectral region from −0.05 to −0.8 ppm decrease their signal intensity with the addition of PA. However, PA has no effect on peaks u2, u6, and other peaks. The most prominent change occurs with peaks u4 and u5.

^{1}H NMR also detects the $–CH_2$ PA peak in the presence of MbCO. Upon the addition of 3.2 mM of PA, the PA $-CH_2$ peak appears at 1.14 ppm, fig 4A–B. The difference spectrum reveals clearly the $–CH_2$ PA peak, fig 4C. The $-CH_2$ of PA in MbCO solution resonates 0.15 ppm upfield from its corresponding 1.29 ppm chemical shift position in Tris buffer at pH 7.4 and 35°C [67].

Fig 5 displays the ^{1}H difference spectra of MbCO with varying MbCO:PA ratios from 1:0 to 1:4. The peak at 0 ppm corresponds to 3.2 mM TSP internal reference. The PA $-CH_2$ peak intensity increases, as PA level increases.

In particular, the signal intensity of u4 and u5 decreases with increasing amount of PA. The signal intensity change reveals a PA dependence that reaches a saturating PA-Mb level and gives rise to an estimate of the apparent dissociation constants of 39 and 48 μM for u4 and u5 respectively, fig 6.

In fig 7, the graph shows the non-specific interaction of PA with MbCO and MbCN, as determined by the area of the NMR visible $–CH_2$ PA signal. Up to 2.2 mM of the PA introduced into either MbCO or MbCN solution, only 41% appears as an NMR detectable signal. Above 2.2 mM, however, the soluble PA fraction no longer increases. Both MbCO and MbCN exhibit a similar non-specific PA interaction profile. The NMR visible PA fraction suggests a 0.8% solubility in Tris [67] . Table 1 tabulates the PA solubility in different Mb solution states.

The NMR spectra of ^{13}C1 PA in MbCO and deoxy Mb also confirm contrasting interactions. Upon the addition of ^{13}C1 PA in MbCO, the ^{13}C spectra show the PA carboxyl group signals appearing at both 172 and 182 ppm, fig 8A–8B. In deoxy Mb, no ^{13}C1 PA signal appears, fig 8C–8D. In Tris buffer at pH 7.4 and 9.5, $^{13}C_1$ PA produces signals at 172 and 184 ppm, respectively, fig 8E–8F.

Bovine serum albumin (BSA) and Mb compete for PA. Fig 9 displays the competitive binding of PA to BSA and Mb. Titrating PA into MbCO produces selective signal intensity changes, most notably in the decrease in peaks u4 and u5, fig 9A–B. However, with the

addition of 0.8 mM bovine serum albumin (BSA), the peaks u4 and u5 recover to their initial intensity, fig 9C.

^{13}C experiments also detect the competitive binding of PA to MbCO and BSA, fig 10. Introducing $^{13}C_1$ PA in MbCO produces the distinct $^{13}C_1$ PA peak at 182 ppm, fig 10A–10B. With the addition of BSA, the PA signal at 182 ppm disappears, and a new peak emerges at 184 ppm, corresponding to PA bound BSA.

The analysis of the $^{13}C_1$ PA signals during the titration of BSA into MbCO-PA reveals an apparent BSA/Mb partition coefficient of 16.5:1, fig 11. Using literature values for the dissociation constant (K_d) of PA bound to the first binding site in BSA (2–147 nM) and the apparent BSA/Mb partition coefficient leads to a corresponding apparent Mb-PA K_d of 0.03–2.4 μM [2,4,5,15,58,62,65,66].

The experimentally determined Mb-PA K_d provides input values to model the intracellular fatty acid flux, Table 2 and equation 1. Curve A in fig 12 models the free fatty acid flux based on PA solubility in Tris. Curve B estimates the FABP mediated fatty acid flux using a cellular FABP concentration of 50 μM, a K_d = 14 nM [21,60]. Curve C models the free fatty acid flux based on the enhanced solubility of PA in the presence of MbCO (41%). Curve D shows that MbCO facilitated transport of PA based on cellular concentration of [Mb]=0.26mM and the apparent K_d=48μM. A Mb-PA K_d=48μM would indicate a Mb facilitated PA flux exceeding the FABP facilitated PA flux at cellular PA concentration above 0.02μM [48,67]. The V_{max} values per g tissue for FABP= 1.5×10^{-7} $nmolcm^2s^{-1}g^{-1}$ and for Mb = 2.0×10^{-4} $nmolcm^2s^{-1}g^{-1}$. The model assumes that deoxy Mb does not bind PA and therefore cannot facilitate PA transport.

Figure 13 models the fatty acid flux at high PA and Mb concentration. Curve A: FABP facilitated fatty acid flux. Curve B: fatty acid flux based on [Mb]= 0.26mM and the apparent K_d=48μM. Curve D shows fatty acid flux based on [Mb]= 3.8mM and the apparent K_d=48μM [48,52]. At high Mb concentration, Mb facilitated PA transport predominates under all conditions and will reach a V_{max} value of 3×10^{-3} $nmolcm^2s^{-1}g^{-1}$ for 3.8 mM Mb observed in marine mammals.

4. DISCUSSION

4.1 Palmitate with MbCO

Previous experiments have shown that the addition of PA to Fe (III) MbCN perturbs selectively the hyperfine shifted 8 heme methyl signal [67]. The observation has led to the hypothesis that Mb can specifically bind fatty acid in localized protein regions. Even though Fe (III) MbCN has served as an analog of the ligated state of Mb, questions still remain about fatty acid interaction with the physiological Fe (II) Mb, which can bind and release O_2 and CO. Indeed, the addition of palmitate produces a selective signal intensity loss in the ^1H NMR spectra of ligated MbCO, consistent with a specific palmitate-protein interaction. Palmitate induces intensity changes in several ring current shifted peaks, most notably u4 and u5. Literature reports have assigned these peaks to Val 17 and Leu 2 [47].

Analysis of the palmitate-MbCO titration curve of u4 leads to the determination of an apparent K_d of 39–48μM, consistent with the MbCN K_d of 12–43μM [67]. The apparent K_d values also agree with previous studies on MbO_2, which shows a lower binding capacity for PA than albumin on a per mole basis [24]. An assay of the competitive binding of PA to Mb and bovine serum albumin (BSA) shows a BSA/Mb partition coefficient of 16.5. BSA competes more effectively for PA than Mb. However, the literature contains many reports of fatty acid binding to BSA with widely varying number of binding sites from 1 to 8 and K_d

values ranging from 2 to 1,000,000 nM [2,4,5,15,58,62,65,66]. Even limiting the K_d values reported for the 1st binding site of BSA still yields a range from 2 to 147 nM. These BSA K_d values and the apparent BSA/Mb partition coefficient of 16.5 would still lead to a wide range of Mb K_d values between 0.03–2.4 μM, which unfortunately precludes a confident assessment of the Mb-PA binding affinity. Nevertheless, the analysis suggests that the NMR calculation overestimates the actual K_d value (vide infra).

4.2 Palmitate with deoxy Mb

In contrast, unligated Fe (II) Mb (deoxygenated Mb) shows no detectable interaction with PA. PA does not perturb any detectable signals from the heme $5CH_3$, 6Hα propionate, 4Hα vinyl, 2Hα vinyl, and 7 Hα propionate, as observed in the hyperfine shifted 10–15 ppm spectral region [6,39]. No hyperfine shifted signals in the upfield region appear perturbed. Given the postulated interaction of fatty acid near the 8 heme methyl, the adjacent 7 Hα propionate group should experience a significant structural perturbation and exhibit spectral alteration. PA does not perturb the NMR observable 7 Hα propionate peak at 11 ppm. The observation stands in sharp contrast to the detectable PA interaction with MbCN and MbCO.

4.3 Non-specific interaction of palmitate with MbCO and deoxy Mb

In addition to the specific interaction, PA interacts non-specifically with MbCO. The non-specific interaction leads to a detectable increase in the PA methylene peak signal, which reflects about a 10^4 times higher PA solubility in the presence of MbCN than in buffer [67]. Associated with a non-specific interaction, the methylene signal of PA in MbCN shifts upfield by 0.15 ppm from its corresponding position observed in buffer [12].

The titration of PA into MbCO induces also a 0.15 ppm upfield shift of the methylene ($-CH_2$) groups of PA. PA in MbCN vs. MbCO yields a comparable $-CH_2$ PA signal intensity. In contrast, deoxy Mb does not exhibit any non-specific interaction with PA and does not enhance the PA solubility at wide range of Mb:PA ratios Upon adding dithionite to the MbCN-PA solution, deoxy Mb forms immediately. The methylene signal of PA disappears, consistent with a loss of non-specific interaction of PA with Mb. Adding dithionite to the buffer solution containing PA also does not alter the PA $-CH_2$ signal intensity nor chemical shift at 1.29 ppm. Dithionite has no effect on either the PA chemical shift or solubility.

4.4 Comparison of interaction with MbCN and MbCO

In many protein structure studies, Fe (III) MbCN has served as a surrogate model of the ligated form of the physiological Fe (II) MbO_2 or MbCO, because the electron-nuclear interaction of the paramagnetic Fe(III) shifts by hyperfine interaction the heme and localized heme pocket amino acid residue signals into observable parts of the NMR spectral window [38]. These signals permit then a sensitive tracking of the interaction between the heme electronic and protein structures. In contrast, detecting the corresponding heme signals in MbO_2 or MbCO poses a technical challenge, since these peaks resonate in a crowded, overlapping spectral region of the diamagnetic Fe(II) protein. Specifically, the heme methyl signals of both MbCO and MbO_2 appear within a diamagnetic region around 3.5 ppm. In particular, the 8 heme methyl signal resonates at 3.59 ppm [6,46].

Because MbCO and MbCN share key structural features, they should exhibit similar specific and non-specific interactions. Indeed, the PA does interact specifically with MbCO and MbCN and shows the same increased PA solubility, which stands well above PA solubility in buffer [67]. Moreover, in the presence of either MbCO or MbCN, the PA $-CH_2$ peak shifts from 1.29 ppm (chemical shift observed in buffer) to 1.14 ppm. Up to 2.2 mM added PA, the soluble PA fraction in MbCO or MbCN increases linearly with a slope of 0.41. Above 2.2 mM added PA, the soluble PA fraction appears to plateau at 9×10^{-4}M. The

maximum solubility appears higher than previously reported for PA in MbCN and arises most likely from a switch in the experiment method, which uses glass rather than plastic pipettes to transfer fatty acid during PA titration [67]. The literature has reported a PA solubility of 3.2×10^{-6}M in water at 30°C and $< 3.2 \times 10^{-6}$M in pH 7.4 phosphate buffer at 37°C, Table 1.

4.5 ^{13}C NMR of PA in Mb

In titrating $^{13}C_1$ PA, two peaks appear immediately in the ^{13}C spectra. The dominant one resonates at 182 ppm, while the broad smaller peak appears at 172 ppm. The 182 ppm signal increases with PA addition well beyond the 1:1 stoichiometric ratio of PA: Mb and appears consistent with a non-specific binding rather than a specific binding of PA to Mb. Comparing the ^{13}C spectra of $^{13}C_1$ PA in buffer at pH 7.4 and 9.5, where the lamellar and micellar form of fatty acid exhibits a $^{13}C_1$ PA signal at 174 ppm and 184 ppm, respectively, suggests that Mb appears to shift the equilibrium between the lamellar and micellar forms of PA toward the micellar form.

4.6. Structural Interaction of Mb with Fatty Acid

The crystallographic view of a closely packed Mb structure seems to preclude any fatty acid binding. However, Mb does exhibit transient fluctuations that open distinct pathways for ligands to migrate from its surrounding to the heme [14]. Specifically, researchers have postulated a specific role for the 6 and 7 heme propionates. Near the heme 6 propionate, Lys 45 (horse Mb) or Arg 45 (sperm whale Mb) regulates purportedly ligand migration from the protein surface to heme [7,40,41]. In sperm whale MbCN, Arg 45 forms hydrogen bonds with the carboxylate of Asp E3 and the 6-propionate. In horse Mb, the short side chain of Lys 45 cannot form hydrogen bonds with both carboxylates. Without the hydrogen bonds, the 6-propionate of horse Mb exhibits a greater mobility than the corresponding propionate of sperm whale Mb, and associated protein region displays less structural features. This enhanced flexibility in the ligated state of Mb has helped to rationalize the difference in ligand K_{on} and K_{off} for horse Mb and sperm whale Mb. In contrast, the 7 propionate remains mobile in both ligated sperm whale and horse Mb, since it has a similar molecular stabilization configuration.

In deoxy Mb, 2D NMR measurements have detected that the 7 propionate exhibits a greater mobility than the 6 propionate group, as reflected by the nuclear Overhauser enhancements (NOEs) from the propionates to the respective 5 and 8 heme methyls [6]. The propionate mobility in different ligation states of Mb influences ligand migration and may also modulate the selective binding of fatty acid [40,41,56]. In the MbCN spectrum, only the 8-heme methyl neighboring the 7-propionate experiences a signal perturbation upon the addition of PA. In the deoxy Mb spectrum, no hyperfine shifted peak exhibits any perturbation.

The PA molecule appears to interact with other regions of Mb, as reflected in the perturbation of the upfield resonances in the MbCO spectra. Neither amino acid residue Val 17 nor Leu 2 (peaks u4 and u5) neighbors the heme 8-methyl group. What gives rise to the contrasting PA interaction requires further investigation.

4.7 Implication for Mb and Intracellular Fatty Acid Transport

Because the cell contains organelles, proteins, and other macromolecules, the fatty acid solubility in buffer may not accurately reflect the actual solubility in the cell. In fact, proteins will most likely have a range of non-specific interactions. A previous study has shown, for example, that lysozyme has no interaction with fatty acid [67].

The contrasting PA interactions with MbCO and deoxy Mb suggest a potential role for Mb in regulating directly fatty acid metabolism. Current model ascribes an exclusive function to FABP as a carrier of intracellular fatty acid. Rat heart contains about 50 μM of FABP with a K_d of 14 nM for fatty acid [21,60]. Despite FABP's high affinity for fatty acid, many unresolved questions still surround the hypothesis that FABP alone facilitates fatty acid transport in the cell [22,44,69,71,75].

At low fatty acid concentration, the high affinity FABP will first bind fatty acid. Fatty acid flux, however, does not depend only upon binding affinity. It also depends upon protein concentration and diffusivity. Rodent heart contains 5 times more Mb (260 μ*M*) than FABP (50 μM) [48,67].

For FABP, the literature has reported a diffusion coefficient in the cell of 3.05×10^{-9} cm^2s^{-1} and a Kd of 14 nM. Consequently, FABP can facilitate fatty acid flux at a maximal rate of 1.5×10^{-7} $nmolcm^2s^{-1}g^{-1}$[45]. Cellular Mb, however, diffuses at 7.85×10^{-7} cm^2s^{-1}. Using the apparent Kd of 48 μM for PA binding to MbCO as the dissociation constant for ligated state of Mb, Mb facilitated fatty acid flux will reach a much higher flux rate of 2.0×10^{-4} $nmolcm^2s^{-1}g^{-1}$ in rat heart and 30×10^{-4} $nmolcm^2s^{-1}g^{-1}$ in seal skeletal muscle. Seal muscle contains about 15 times more myoglobin than rodent muscle.

Because all PA does not necessarily dissolve in the Mb solution, the apparent K_d calculation most likely overestimates the actual value. The BSA-PA partition coefficient analysis also suggests a lower K_d. A lower K_d implies that Mb will exceed FABP in transporting fatty acid at a lower cellular fatty acid concentration. Future studies using other approaches, such as fluorometric and isothermal calorimetry techniques, will provide additional clarification of the K_d value. Regardless of the K_d, however, Mb appears to have a much higher capacity to transport fatty acid in the cell.

4.8 A Model of Intracellular Fatty Acid Transport

In principle, the intracellular fatty acid flux has contributions from carrier mediated transport and free diffusion. Because PA solubility increases appreciably in the presence of Mb, the free fatty acid would contribute much more than its solubility in buffer might suggest. In buffer, the low solubility would appear to militate against any significant contribution of free fatty acid. In Mb solution, however, PA solubility increases dramatically.

Moreover, because MbCN and MbCO interact non-specifically with PA in a similar way, it suggests that MbO_2 can influence the available fatty acid pool and the capacity to transport PA in the cell. In contrast, when Mb becomes deoxygenated, its capacity to interact with fatty acid diminishes. As a consequence, fatty acid availability would have a dependence on cellular partial pressure of oxygen (PO_2), especially along a PO_2 gradient from the sarcolemma near the capillary to the mitochondria, where fatty oxidation occurs and where cytochrome oxidase operates at a purported Km of about 0.1 mm Hg of PO_2 [37,74]. The contrasting O_2 dependent Mb affinity for fatty acid presents a convenient mechanism to load and unload fatty acid at different cellular sites, depending upon the PO_2 environment and the Mb oxygenation state.

Imputing a fatty acid transport role for Mb agrees with previous observations, which found ^{14}C labeled oleic acid binding to a rat heart cytosolic fraction of 16 kD molecular weight, which includes both Mb and FABP [26,63]. Because Mb has an approximately 3,000 times lower binding affinity than FABP and lower binding affinity than albumin, the role of Mb as a fatty acid transport might appear surprising. However, the high fatty acid affinity for FABP in the current model of intracellular fatty acid transporter requires potentially a complex mechanism to release fatty acid at the metabolism site [13]. In

contrast, the high Mb concentration relative to the low FABP concentration and the Mb fatty acid affinity shifting with respect to PO_2 might enable Mb to compete effectively with FABP to transport fatty acid transport [24,67].

Given the proposed model of Mb facilitated fatty acid transport, FABP would initially bind PA in the cell and serve as the major transporter below 0.02 μM PA. In all cases, the V_{max} per g tissue for FABP (1.5×10^{-7} $nmolcm^2s^{-1}g^{-1}$) falls far below the corresponding Vmax for Mb (2.0×10^{-4} $nmolcm^2s^{-1}g^{-1}$). The contrasting Vmax values arise in part from the higher concentration of Mb (260 uM) over FABP (50 uM).

Indeed, Mb dependent transport of lipid would certainly broaden the cell's ability to meet a range of metabolic demands for fatty acid and would suggest an alternative explanation of how exercise induced increase in Mb concentration could potentially modulate metabolism [1,64].

4.9 Physiological implication of Mb facilitated fatty acid transport

The Mb facilitated flux of fatty acid would significantly impact cellular bioenergetics during a continuous demand for fatty acid oxidation, especially with respect to trained and untrained muscle. Energy generation relies more on lipid than carbohydrate below the crossover point of about 70% whole body maximum rate of oxygen consumption (VO_{2max}) and during postexercise recovery [3]. Training shifts the crossover point to a higher relative VO_{2max}. Most researchers ascribe the capacity to utilize fatty acid at a higher relative VO_{2max} or exercise intensity to an increase in mitochondrial mass, which would support increased fatty acid oxidation [31–33,49]. Training, however, also appears to increase the Mb concentration, which conventional analysis would view as an increased O_2 transport capacity [1,30]. Since neither *in vivo* NMR nor fluorometric experiments have observed convincing data to show that Mb diffusion can compete effectively with free O_2, Mb dependent fatty acid transport might offer an alternative explanation of how Mb can expand fatty acid utilization in trained muscle [42,43,50,51] .

Even at the beginning of muscle contraction, fatty acid bound to Mb might play a significant role. ^1H NMR studies have noted a rapid desaturation of Mb at the initiation of contraction, and the analysis of the kinetics indicates a sudden rise in intracellular oxygen consumption [11]. A rapid formation of deoxy Mb from MbO_2 would also imply a quick release of fatty acid to fuel ATP formation. A sudden surge in fatty acid utilization at the initiation of contraction, however, seems odd given the common notion that carbohydrate metabolism proceeds much faster than fatty acid metabolism.

For marine mammals, the Mb concentration in skeletal muscle can rise to 3.8 mM. Mb dependent fatty acid flux probably dominates under all physiological conditions [52,53]. In rodent heart, Mb reaches only 0.26 mM and can support only a fatty acid flux of 2.04×10^{-4} $nmolcm^2s^{-1}g^{-1}$ [48]. In contrast, Mb dependent fatty acid flux in the skeletal muscle of seal can rise to 30×10^{-4} $nmolcm^2s^{-1}g^{-1}$.

Mb dependent fatty acid transport may have a unique role in diving mammals. In contrast to common misconception, seals holding their breath during a prolonged dive do not exhibit any sign of anaerobiosis, as indicated by significant lactate washout in the blood [8]. They still rely on oxidative fatty acid metabolism. In eupnea-apnea cycle studies of elephant seals (*M. angustirostris*), a model of diving physiology, the blood does supply during eupnea an adequate amount of O_2 to saturate at least 90% of the cellular MbO_2 [53]. During apnea, the seal spontaneously holds its breath between 8–12 min, and the muscle releases its Mb oxygen store. But the intracellular O_2 level falls only modestly and still saturates Mb at 80%. A reduced cellular O_2 level doesn't necessarily presage anaerobic metabolism,

consistent with recent discussion on the bioenergetics of muscle contraction [11,34]. Indeed during the breath hold in apnea, the cell still remains sufficiently aerobic. PCr and ATP stay at a constant level. PH doesn't change. Lactate formation does not increase. During a breath hold, seal muscle still maintains a highly saturated MbO_2, which can still support fatty transport for oxidative metabolism.

Nevertheless, how Mb contributes to the cell's fuel source selection, as suggested by the findings in this report, remains an open question that requires further investigation.

5. CONCLUSIONS

The ^1H NMR analysis reveals that PA interacts specifically and non-specifically with MbCO. It does not interact with deoxy Mb. Given the diffusion coefficient in the cell, cellular concentration, and the assumption of an identical K_d for MbO_2 as for MbCO, a model of intracellular fatty acid transport indicates that Mb mediated fatty acid diffusion could contribute significantly. Moreover, the differential PA interaction with Mb with respect to PO_2 suggests a convenient mechanism to load and unload PA.

Acknowledgments

We gratefully acknowledge funding support from NIH GM 58688 (TJ) and Philip Morris 005510 (TJ) and also the scientific discussion as well as assistance of Dr. Ulrike Kreutzer.

Abbreviations

PA	palmitate
FABP	fatty acid binding protein
Mb	myoglobin
MbCO	carbonmonoxy myoglobin

References

1. Beyer R, Fattore J. The influence of age and endurance exercise on the myoglobin concentration of skeletal muscle of the rat. Journal of Gerontology. 1984; 39:525–530.
2. Bojesen IN, Bojesen E. Water-phase palmitate concentrations in equilibrium with albumin-bound palmitate in a biological system. J. Lipid Res. 1992; 33:1327–1334.
3. Brooks GA, Mercier J. Balance of carbohydrate and lipid utilization during exercise: the "crossover" concept. J. Appl Physiol. 1994; 76:2253–2261.
4. Burczynski FJ, Cai ZS. Palmitate uptake by hepatocyte suspensions: effect of albumin. Am. J. Physiol. 1994; 267:G371–G379.
5. Burczynski FJ, Cai ZS, Moran JB, Forker EL. Palmitate uptake by cultured hepatocytes: albumin binding and stagnant layer phenomena. Am. J. Physiol. 1989; 257:G584–G593.
6. Busse SC, Jue T. Two-dimensional NMR characterization of the deoxymyoglobin heme pocket. Biochemistry. 1994; 33:10934–10943.
7. Carver TE, Olson JS, Smerdon SJ, Krzywda S, Wilkinson AJ, Gibson QH, Blackmore RS, Ropp JD, Sligar SG. Contributions of residue 45(CD3) and heme-6-propionate to the biomolecular and geminate recombination reactions of myoglobin. Biochemistry. 1991; 30:4697–4705.
8. Castellini MA, Milsom WK, Berger RJ, Costa DP, Jones DR, Castellini JM, Rea LD, Bharma S, Harris M. Patterns of respiration and heart rate during wakefulness and sleep in elephant seal pups. Am. J. Physiol. 1994; 266:R863–R869.
9. Chung Y, Huang SJ, Glabe A, Jue T. Implication of CO inactivation on myoglobin function. Am. J. Physiol Cell Physiol. 2006; 290:C1616–C1624.

10. Chung Y, Jue T. Cellular response to reperfused oxygen in the postischemic myocardium. Am J Physiol. 1996; 271:H687–H695.
11. Chung Y, Mole PA, Sailasuta N, Tran TK, Hurd R, Jue T. Control of respiration and bioenergetics during muscle contraction. Am J Physiol Cell Physiol. 2005; 288:C730–C738.
12. Cistola DP, Walsh MT, Corey RP, Hamilton JA, Brecher P. Interactions of Oleic-Acid with Liver Fatty-Acid Binding-Protein - A C-13 Nmr-Study. Biochemistry. 1988; 27:711–717.
13. Corsico B, Liou HL, Storch J. The alpha-helical domain of liver fatty acid binding protein is responsible for the diffusion-mediated transfer of fatty acids to phospholipid membranes. Biochemistry. 2004; 43:3600–3607.
14. Elber R, Karplus M. Multiple conformational states of proteins: a molecular dynamics analysis of myoglobin. Science. 1987; 235:318–321. [PubMed: 3798113]
15. Elmadhoun BM, Wang GQ, Templeton JF, Burczynski FJ. Binding of [3H]palmitate to BSA. Am. J. Physiol. 1998; 275:G638–G644.
16. Emerson SD, La Mar G. Solution structural characteristics of cyanometmyoglobin: resonance assignment of heme cavity residues by two-dimensional NMR. Biochemistry. 1990; 29:1545–1556.
17. Flogel U, Laussmann T, Godecke A, Abanador N, Schafers M, Fingas CD, Metzger S, Levkau B, Jacoby C, Schrader J. Lack of myoglobin causes a switch in cardiac substrate selection. Circ Res. 2005; 96:e68–e75.
18. Flogel U, Merx MW, Godecke A, Decking UKM, Schrader J. Myoglobin: A scavenger of bioactive NO. Proc. Natl. Acad. Sci. 2001; 98:735–740.
19. Garry DJ, Ordway GA, Lorenz JN, Radford NB, Chin ER, Grange RW, Bassel-Duby R, Williams RS. Mice without myoglobin. Nature. 1998; 395:905–908.
20. Glabe A, Chung Y, Xu D, Jue T. Carbon monoxide inhibition of regulatory pathways in myocardium. Am J Physiol. 1998; 274:H2143–H2151.
21. Glatz JF, Schaap FG, Binas B, Bonen A, van der Vusse GJ, Luiken JJ. Cytoplasmic fatty acid-binding protein facilitates fatty acid utilization by skeletal muscle. Acta Physiol Scand. 2003; 178:367–371.
22. Glatz JF, Schaap FG, Binas B, Bonen A, van der Vusse GJ, Luiken JJ. Cytoplasmic fatty acid-binding protein facilitates fatty acid utilization by skeletal muscle. Acta Physiol Scand. 2003; 178:367–371.
23. Glatz JF, van der Vusse GJ. Intracellular transport of lipids. Mol. Cell Biochem. 1989; 88:37–44. [PubMed: 2674666]
24. Glatz JFC, Veerkamp JH. A Radiochemical Procedure for the Assay of Fatty-Acid Binding by Proteins. Anal. Biochem. 1983; 132:89–95.
25. Gloster J. Studies on Fatty-Acid Binding Characteristics of Myoglobin and Z-Protein. J. Molec. Cell Cardiol. 1977; 9:15.
26. Gloster J, Harris P. Fatty-Acid Binding to Cytoplasmic Proteins of Myocardium and Red and White Skeletal-Muscle in Rat - Possible New Role for Myoglobin. Biochem. Biophys. Res. Comm. 1977; 74:506–513.
27. Godecke A, Flogel U, Zanger K, Ding Z, Hirchenhain J, Decking UK, Schrader J. Disruption of myoglobin in mice induces multiple compensatory mechanisms. Proc. Natl. Acad. Sci. U. S. A. 1999; 96:10495–10500.
28. Gotz FM, Hertel M, Groschelstewart U. Fatty-Acid-Binding of Myoglobin Depends on Its Oxygenation. Biological Chemistry Hoppe-Seyler. 1994; 375:387–392.
29. Gros G, Wittenberg B, Jue T. Myoglobin's old and new clothes: from molecular structure to function in living cells. J. Exp. Biol. 2010; 213:2713–2725.
30. Harms SJ, Hickson RC. Skeletal muscle mitochondria and myoglobin, endurance, and intensity of training. J. Appl. Physiol. 1983; 54:798–802.
31. Henriksson J, Reitman JS. Time course of changes in human skeletal muscle succinate dehydrogenase and cytochrome oxidase activities and maximal oxygen uptake with physical activity and inactivity. Acta Physiol Scand. 1977; 99:91–97.

32. Holloszy JO. Biochemical adaptations in muscle. Effects of exercise on mitochondrial oxygen uptake and respiratory enzyme activity in skeletal muscle. J. Biol. Chem/. 1967; 242:2278–2282.
33. Holloszy JO, Coyle EF. Adaptations of skeletal muscle to endurance exercise and their metabolic consequences. J. Appl Physiol. 1984; 56:831–838.
34. Jue, T. Bioenergetics Implication of Metabolic Fluctuation During Muscle Contraction. In: Shulman, RG.; Rothman, DL., editors. Metabolomics by in vivo NMR. Chichester: John Wiley & Sons, Ltd; 2004. p. 104-117.
35. Kreutzer U, Jue T. Investigation of bioactive NO-scavenging role of myoglobin in myocardium. Eur J Physiol. 2006; 452:36–42.
36. Kreutzer U, Chung Y, Butler D, Jue T. ^{1}H-NMR characterization of the human myocardium myoglobin and erythrocyte hemoglobin signals. Biochim. Biophys. Acta. 1993; 1161:33–37.
37. Kreutzer U, Jue T. The role of myoglobin as a scavenger of cellular NO in myocardium. Am J Physiol. 2004; 286:H985–H991.
38. La Mar, GN. Model Compounds As Aids in Interpreting NMR Spectra of Hemoproteins. In: Shulman, RG., editor. Biological Applications of Magnetic Resonance. New York: Academic Press; 1979. p. 305-343.
39. La Mar GN, Davis NL, Johnson RD, Smith WS, Hauksson JB, Budd DL, Dalichow F, Langry KC, Morris IK, Smith KM. Nuclear magnetic resonance investigation of the electronic structure of deoxymyoglobin. J. Am. Chem Soc. 1993; 115:3869–3876.
40. La Mar GN, Viscio DB, Gersonde K, Sick H. Proton nuclear magnetic resonance study of the rotational position and oscillatory mobility of vinyl groups in allosteric monomeric insect hemoglobins. Biochemistry. 1978; 17:361–367.
41. Lecomte JT, La Mar GN. 1H NMR study of labile proton exchange in the heme cavity as a probe for the potential ligand entry channel in myoglobin. Biochemistry. 1985; 24:7388–7395.
42. Lin PC, Kreutzer U, Jue T. Anisotropy and temperature dependence of myoglobin translational diffusion in myocardium: implication on oxygen transport and cellular architecture. Biophy J. 2007; 92:2608–2620.
43. Lin PC, Kreutzer U, Jue T. Myoglobin translational diffusion in myocardium and its implication on intracellular oxygen transport. J Physiol. 2007; 578:595–603.
44. Luxon BA, Milliano MT. Cytoplasmic codiffusion of fatty acids is not specific for fatty acid binding protein. Am. J. Physiol. 1997; 273:C859–C867. [PubMed: 9316406]
45. Luxon BA, Weisiger RA. Sex-Differences in Intracellular Fatty-Acid Transport -Role of Cytoplasmic-Binding Proteins. Am. J. Physiol. 1993; 265:G831–G841.
46. Mabbutt BC, Wright PE. Assignment of heme and distal amino acid resonances in the 1H- NMR spectra of the carbon monoxide and oxygen complexes of sperm whale myoglobin. Biochim. Biophys. Acta. 1985; 832:175–185. [PubMed: 4063376]
47. Mabbutt BC, Wright PE. Assignment of heme and distal amino acid resonances in the 1H–NMR spectra of the carbon monoxide and oxygen complexes of sperm whale myoglobin. Biochim. Biophys. Acta. 1985; 832:175–185.
48. Masuda K, Truscott K, Lin PC, Kreutzer U, Chung Y, Sriram R, Jue T. Determination of myoglobin concentration in blood-perfused tissue. Eur. J. Appl. Physiol. 2008; 104:41–48.
49. Mole PA, Oscai LB, Holloszy JO. Adaptation of muscle to exercise. Increase in levels of palmityl Coa synthetase, carnitine palmityltransferase, and palmityl Coa dehydrogenase, and in the capacity to oxidize fatty acids. J. Clin. Invest. 1971; 50:2323–2330.
50. Papadopoulos S, Endeward V, Revesz-Walker B, Jurgens KD, Gros G. Radial and longitudinal diffusion of myoglobin in single living heart and skeletal muscle cells. Proc. Natl. Acad. Sci. USA. 2001; 98:5904–5909.
51. Papadopoulos S, Jurgens KD, Gros G. Diffusion of myoglobin in skeletal muscle cells - dependence on fibre type, contraction and temperature. Pflugers Arch. Eur. J. Physiol. 1995; 430:519–525.
52. Ponganis PJ, Kreutzer U, Sailasuta N, Knower T, Hurd R, Jue T. Detection of myoglobin desaturation in Mirounga angustirostris during apnea. Am. J. Physiol Regul. Integr. Comp Physiol. 2002; 282:R267–R272.

53. Ponganis PJ, Kreutzer U, Stockard TK, Lin PC, Sailasuta N, Tran TK, Hurd R, Jue T. Blood flow and metabolic regulation in seal muscle during apnea. J Exp Biol. 2008; 211:3323–3332.
54. Quast K. Flotation of hematite using C6-C18 saturated fatty acids. Minerals Engineering. 2005; 19:582–597.
55. Ralston AW, Hoerr CW. The solubilities of the normal saturated fatty acids. Journal of Organic Chemistry. 1942; 7:546–555.
56. Ramaprasad S, Johnson RD, La Mar GN. Journal of the American Chemical Society. 1984; 106:3632–3635.
57. Rassaf T, Flogel U, Drexhage C, Hendgen-Cotta U, Kelm M, Schrader J. Nitrite reductase function of deoxymyoglobin: oxygen sensor and regulator of cardiac energetics and function. Circ. Res. 2007; 100:1749–1754.
58. Richieri GV, Anel A, Kleinfeld AM. Interactions of long-chain fatty acids and albumin: determination of free fatty acid levels using the fluorescent probe ADIFAB. Biochemistry. 1993; 32:7574–7580.
59. Richieri GV, Ogata RT, Kleinfeld AM. Equilibrium constants for the binding of fatty acids with fatty acid-binding proteins from adipocyte, intestine, and liver measured with the fluorescent probe ADIFAB. J. Biol. Chem. 1994; 269:23918–23930.
60. Richieri GV, Ogata RT, Kleinfeld AM. Kleinfeld, Equilibrium-Constants for the Binding of Fatty-Acids with Fatty-Acid-Binding Proteins from Adipocyte, Intestine, Heart, 1and Liver Measured with the Fluorescent-Probe Adifab. J. Biol. Chem. 1994; 269:23918–23930.
61. Robb ID. Determination of the aqueous solubility of fatty acids and alcohols. Aust. J. Chem. 1966; 19:2281–2284.
62. Rose H, Conventz M, Fischer Y, Jungling E, Hennecke T, Kammermeier H. Long-chain fatty acid-binding to albumin: re-evaluation with directly measured concentrations. Biochim. Biophys. Acta. 1994; 1215:321–326.
63. Said B, Schulz H. Fatty-Acid Binding-Protein from Rat-Heart - the Fatty-Acid Binding-Proteins from Rat-Heart and Liver Are Different Proteins. J. Biol. Chem. 1984; 259:1155–1159. [PubMed: 6420401]
64. Savage DB, Petersen KF, Shulman GI. Disordered lipid metabolism and the pathogenesis of insulin resistance. Physiol Rev. 2007; 87:507–520.
65. Spector AA, Fletcher JE, Ashbrook JD. Analysis of long-chain free fatty acid binding to bovine serum albumin by determination of stepwise equilibrium constants. Biochemistry. 1971; 10:3229–3232.
66. Spector AA, John K, Fletcher JE. Binding of long-chain fatty acids to bovine serum albumin. J. Lipid Res. 1969; 10:56–67.
67. Sriram R, Kreutzer U, Shih L, Jue T. Interaction of fatty acid with myoglobin. FEBS Lett. 2008; 582:3643–3649.
68. Vork MM, Glatz JF, van der Vusse GJ. On the mechanism of long chain fatty acid transport in cardiomyocytes as facilitated by cytoplasmic fatty acid-binding protein. J. Theor. Biol. 1993; 160:207–222.
69. Vork MM, Glatz JF, van der Vusse GJ. Modelling intracellular fatty acid transport: possible mechanistic role of cytoplasmic fatty acid-binding protein. Prostaglandins Leukot. Essent. Fatty Acids. 1997; 57:11–16. [PubMed: 9250602]
70. Vorum H, Madsen P, Svendsen I, Celis JE, Honore B. Expression of recombinant psoriasis-associated fatty acid binding protein in Escherichia coli: Gel electrophoretic characterization, analysis of binding properties and comparison with human serum albumin. Electrophoresis. 1998; 19:1793–1802.
71. Weisiger RA, Zucker SD. Transfer of fatty acids between intracellular membranes: roles of soluble binding proteins, distance, and time. Am. J. Physiol Gastrointest. Liver Physiol. 2002; 282:G105–G115.
72. Wittenberg BA, Wittenberg JB. Transport of oxygen in muscle. Annu. Rev. Physiol. 1989; 51:857–878.
73. Wittenberg JB, Wittenberg BA. Myoglobin function reassessed. J Exp. Biol. 2003; 206:2011–2020. [PubMed: 12756283]

74. Zhang J, Duncker DJ, Xu Y, Zhang Y, Path G, Merkel H, Hendrich K, From AHL, Bache RJ, Ugurbil K. Transmural bioenergetic responses of normal myocardium to high workstates. Am. J. Physiol. 1995; 268:H1891–H1905.

75. Zucker SD. Kinetic model of protein-mediated ligand transport: influence of soluble binding proteins on the intermembrane diffusion of a fluorescent fatty acid. Biochemistry. 2001; 40:977–986.

Research Highlights

- PA interacts specifically and non-specifically with MbCO.
- PA does not appear to interact specifically or non-specifically with deoxy Mb.
- Mb spectral change provides a basis to determine an apparent K_d.
- A model indicates that Mb can compete with FABP to transport fatty acid.

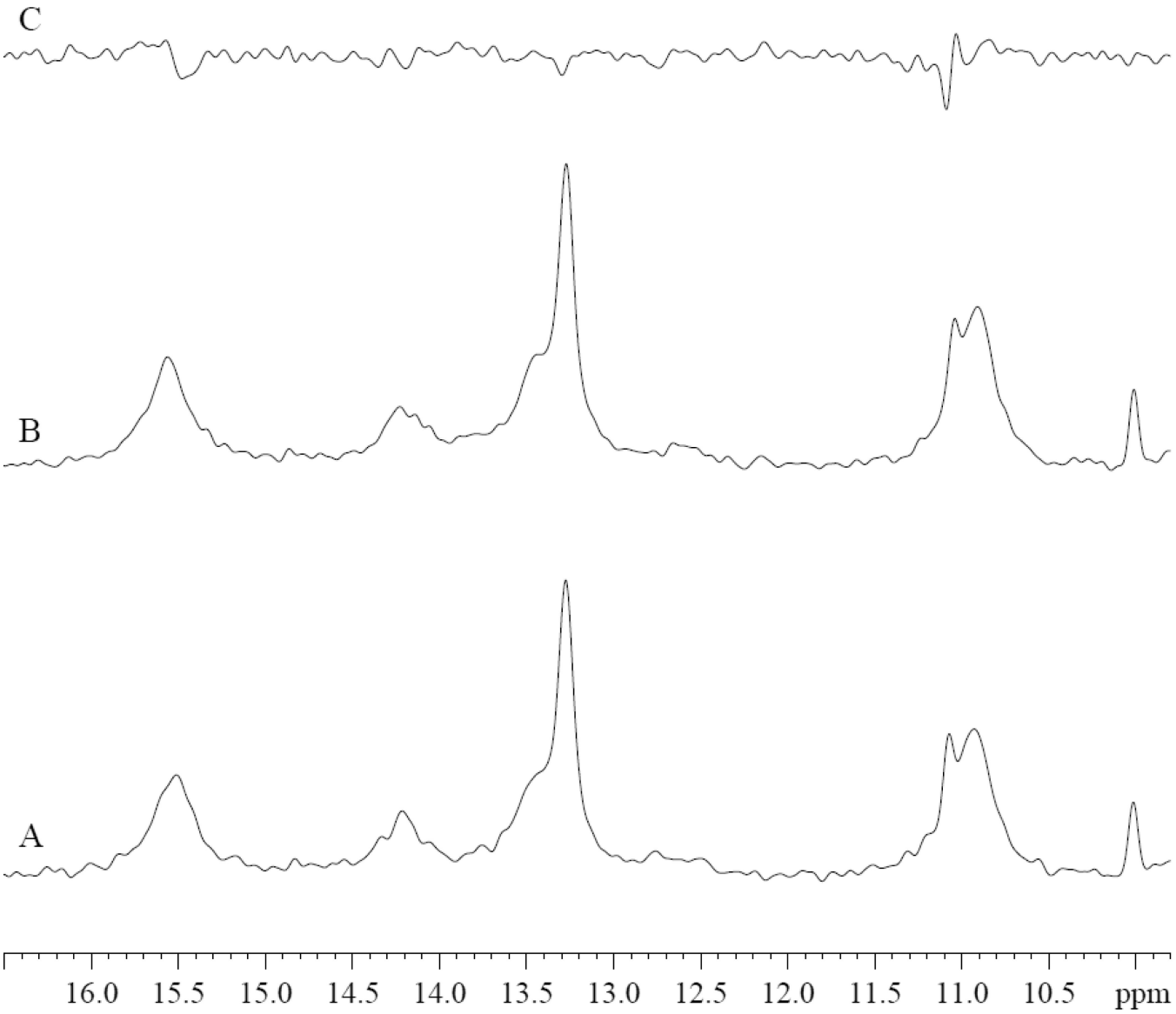

Figure 1.
^{1}H NMR Spectra of hyperfine shifted region of deoxyMb Tris buffer at pH 7.4 at 35°C: A. 0.8mM deoxyMb. B. 0.8mM deoxyMb and 3.2 mM PA. C. difference of B-A.

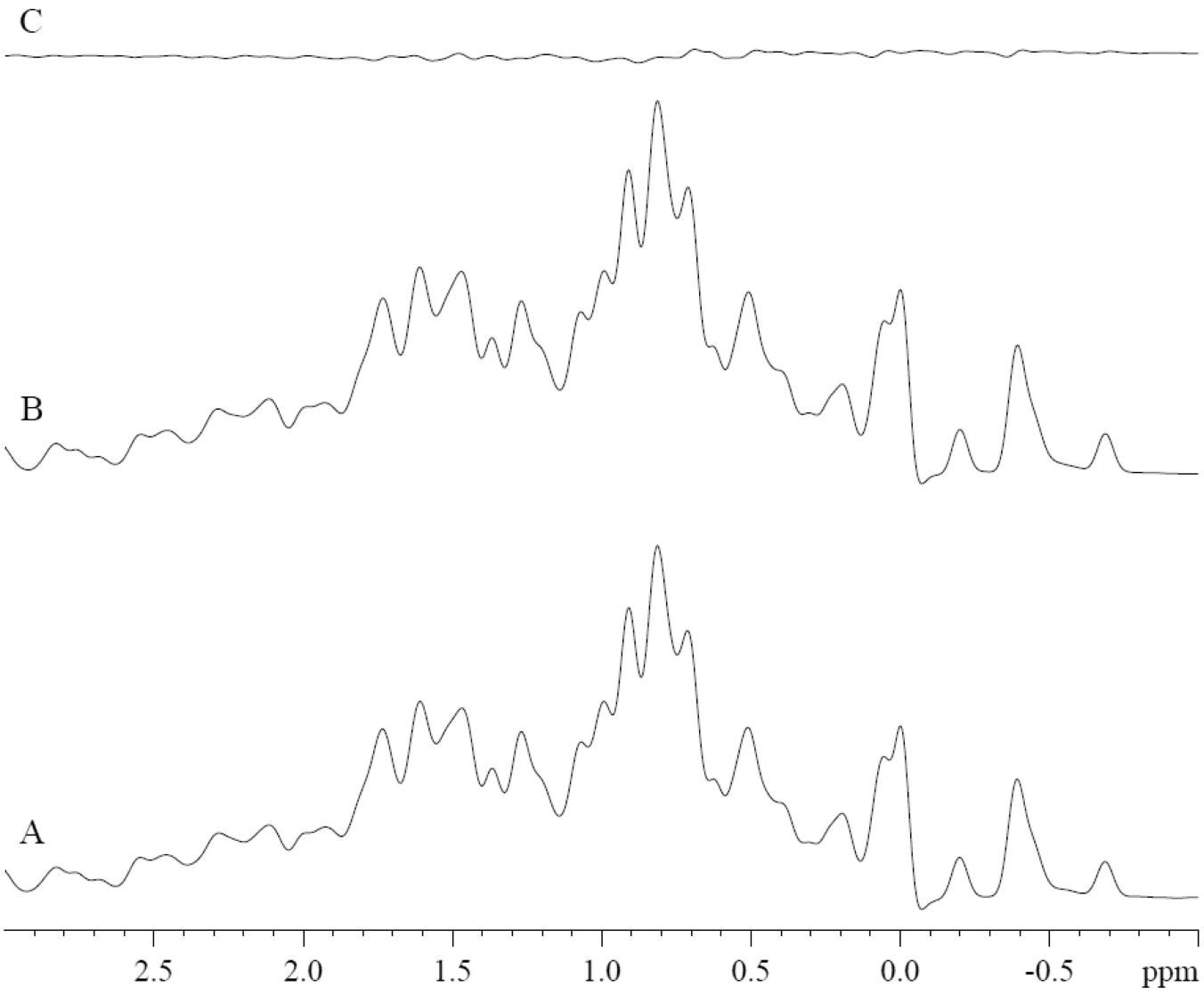

Figure 2.
^{1}H NMR spectra of 0.8mM deoxyMb in Tris buffer at pH 7.4 at 35°C: Spectra of A. 0.8mM deoxyMb B. 0.8mM deoxyMb and 3.2mM PA, C. difference of B-A.

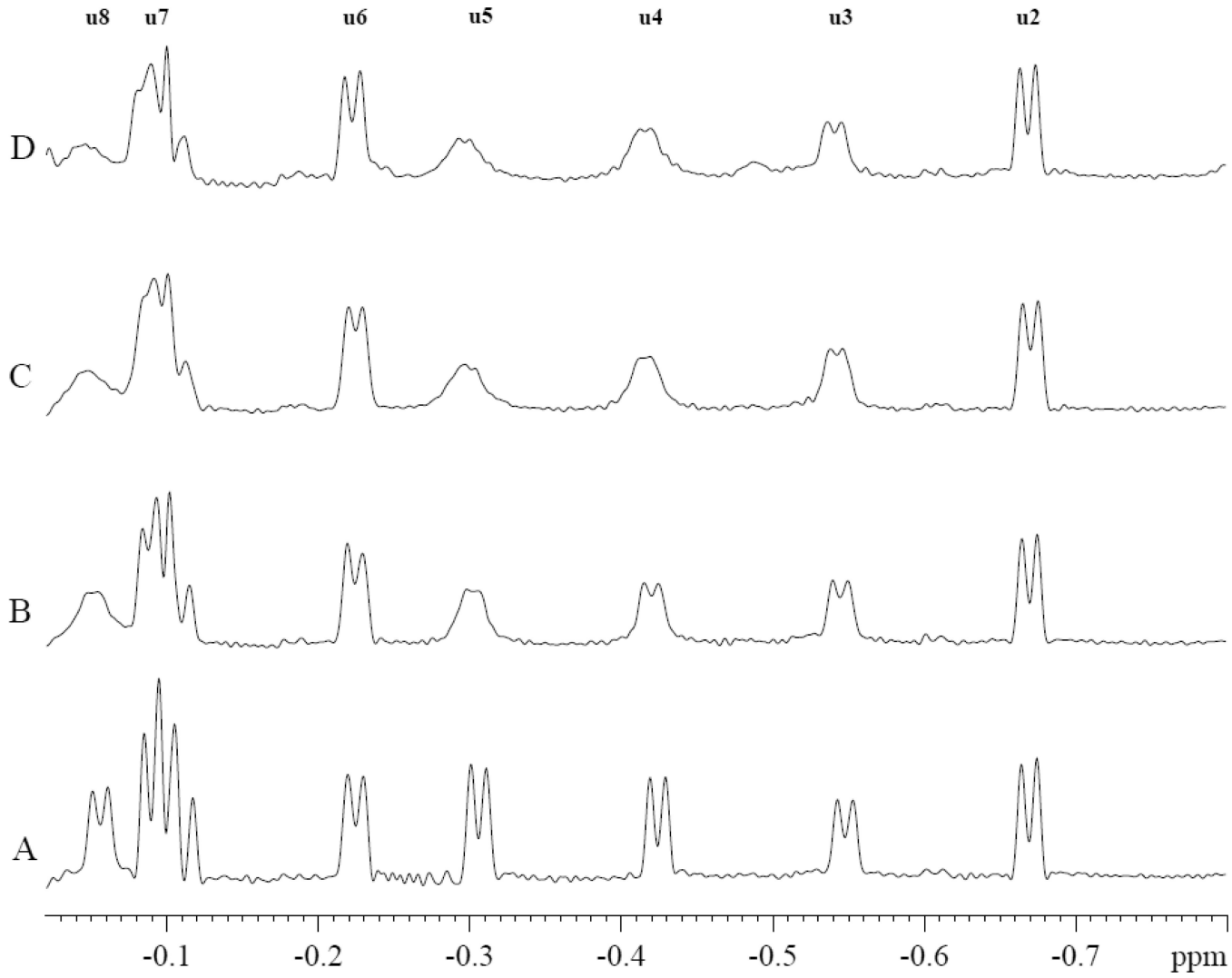

Figure 3.

PA perturbs specifically the MbCO hyperfine shifted ^{1}H NMR peaks (u3, u4, u5, u7, and u8) in the spectral region from −0.05 to −0.8 ppm. PA has no effect on peaks u2, u6, and other peaks. The spectra show the signals from 0.8 mM MbCO with and without palmitate in 30mM Tris and 1mM EDTA buffer with 3.2mM TSP at pH 7.4 and 35°C. A). No PA, B. MbCO:PA=1:0.38, C). MbCO:PA=1:1.9, D). MbCO:PA=1:3.8.

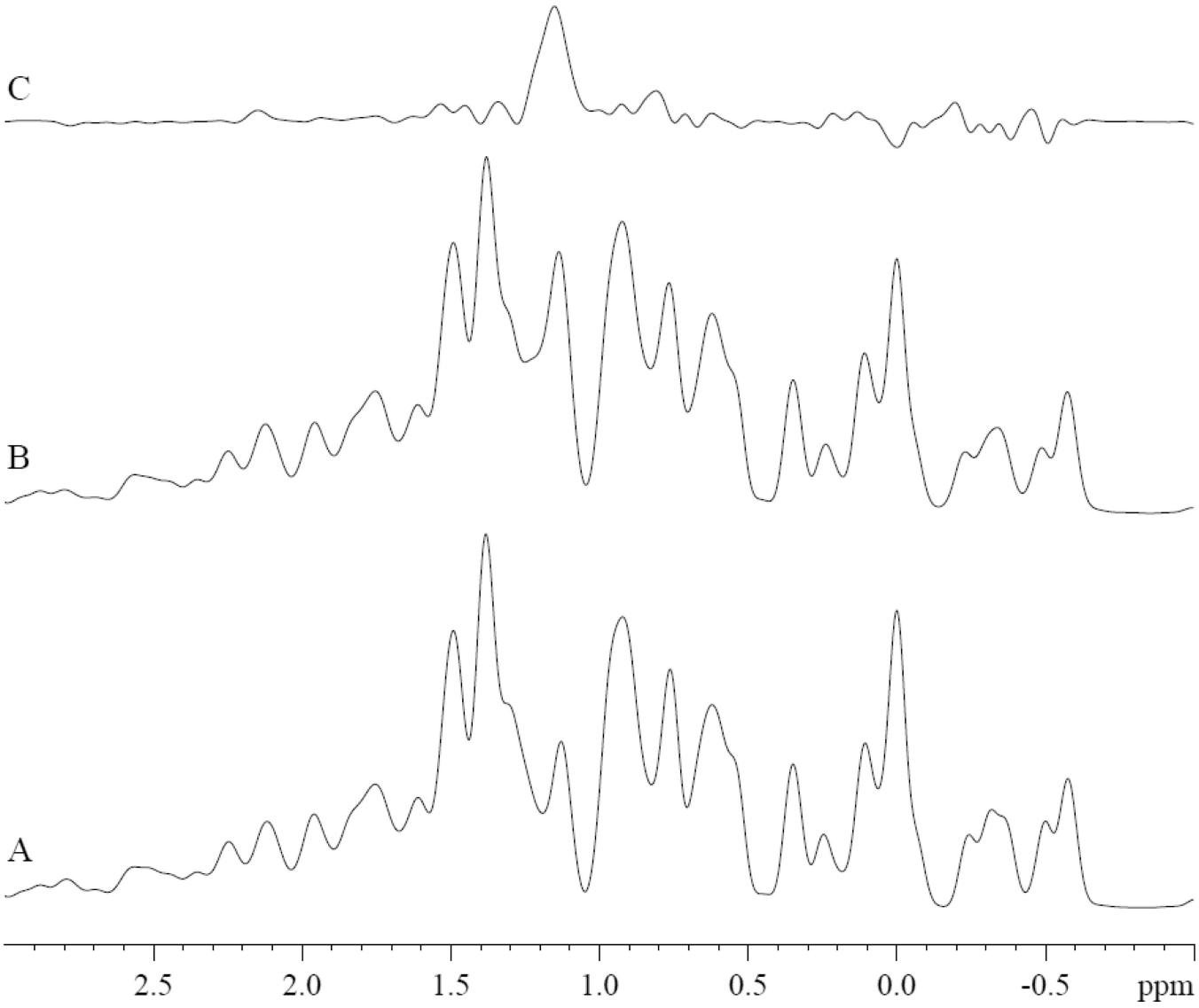

Figure 4.

^{1}H NMR spectra of A) MbCO, B) MbCO with 3.2 mM PA, and C) difference spectrum (B-A). The PA -CH_2 peak appears at 1.14 ppm, 0.15 ppm upfield from its 1.29 ppm chemical shift in Tris buffer at pH 7.4 and 35°C [67].

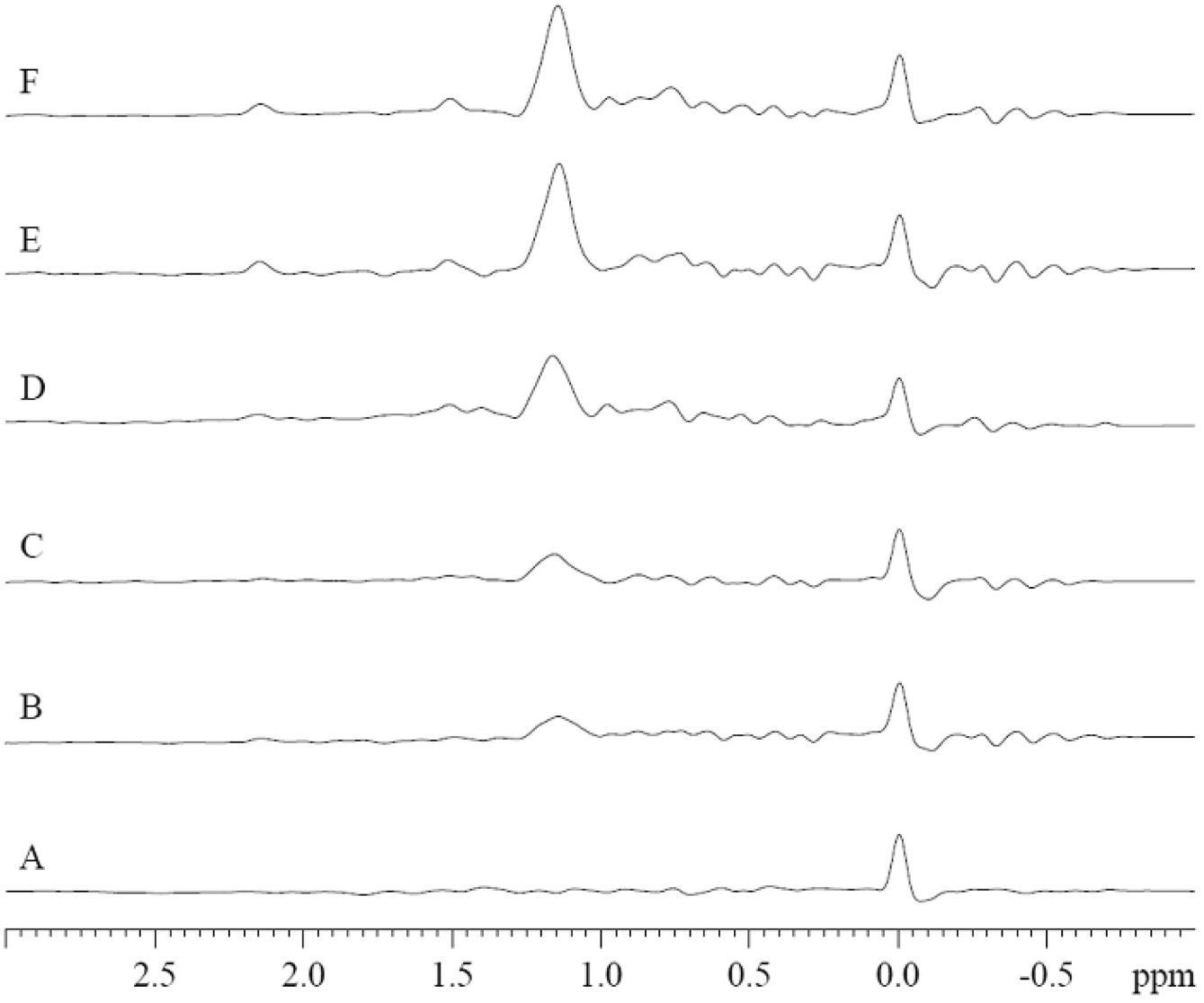

Figure 5.

^{1}H NMR difference spectra of MbCO (MbCO with varying amount of PA and TSP –MbCO without PA and TSP) in 30mM Tris buffer and with 1mM EDTA and with and without 3.2mM TSP at pH of 7.4 at 35°C at varying Mb:PA ratio: A). MbCO:PA=1:0, B). MbCO:PA=1:0.5, C). MbCO:PA=1:1, D). MbCO:PA=1:2, E). MbCO:PA=1:3.5, F). MbCO:PA=1:4. The peak at 0 ppm corresponds to 3.2 mM TSP. The PA -CH_2 peak intensity increases, as PA level increases.

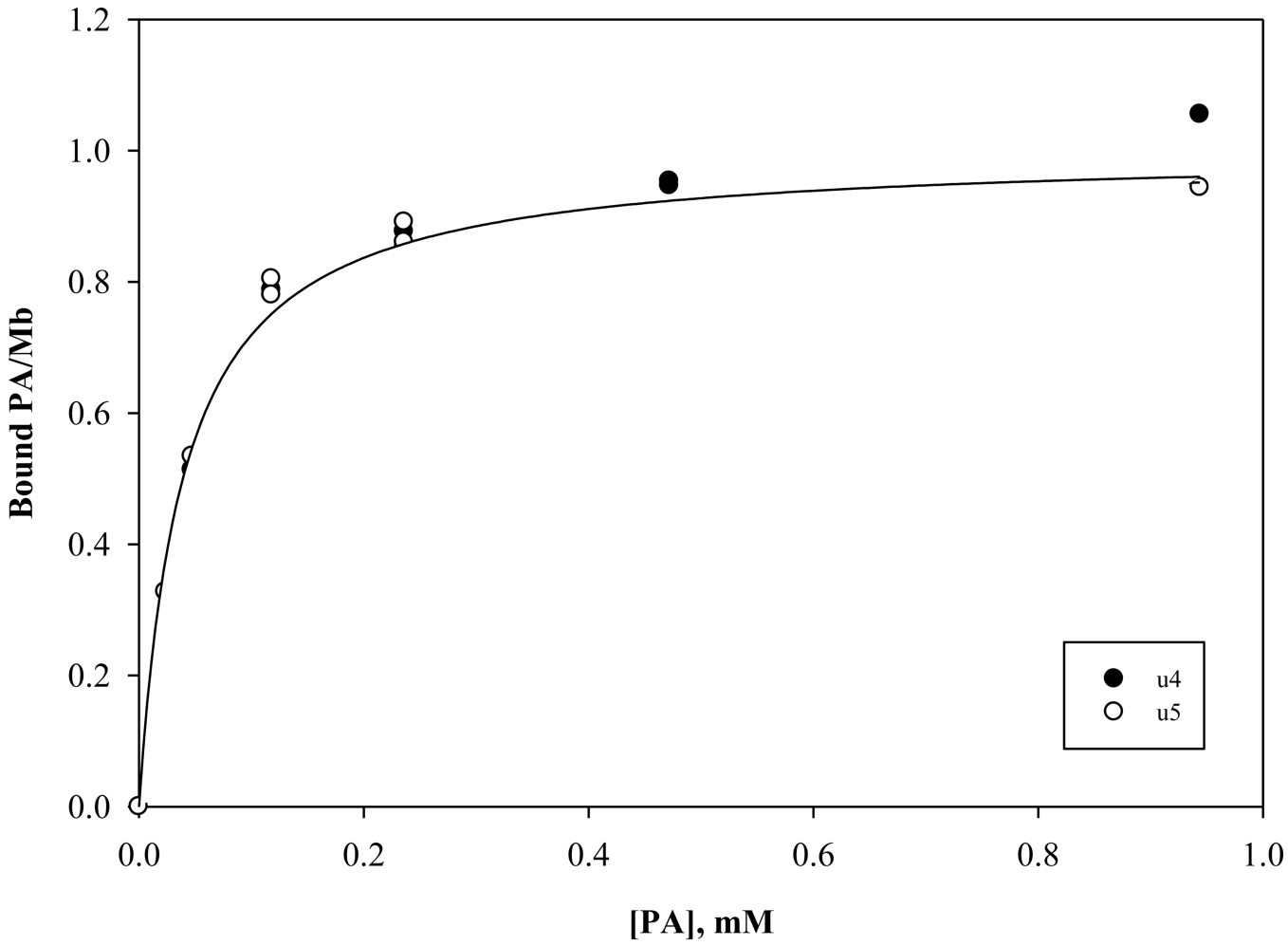

Figure 6.
The signal intensity graph of u4 and u5 during a PA titration reveals a concentration dependence that reaches a saturating PA-Mb level. The analysis of these curves yields apparent dissociation constants 39 and 48 μM for u4 and u5 respectively.

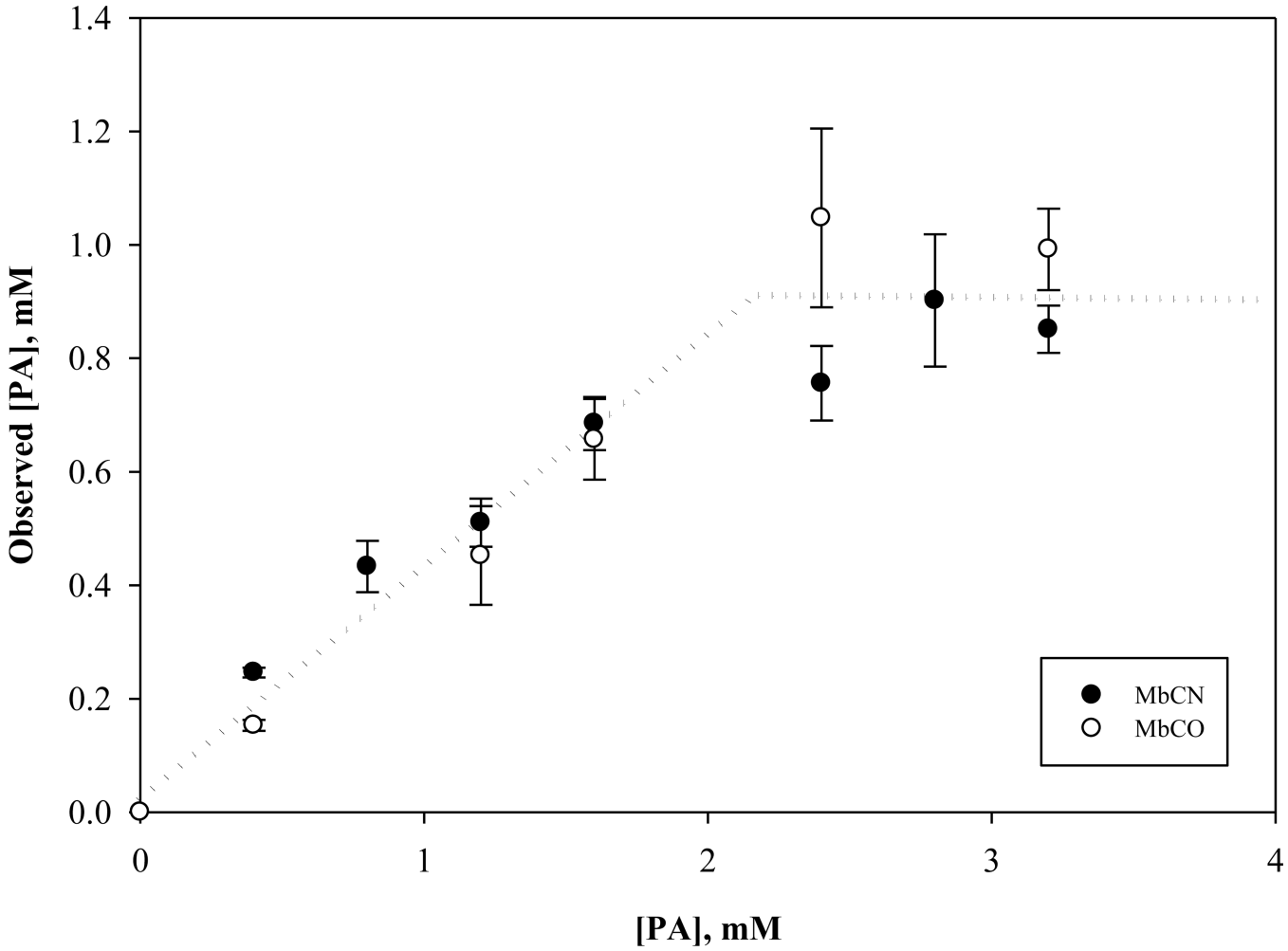

Figure 7.

Graph of the observed PA as a function of actual PA titrated into 0.8 mM MbCN and MbCO in Tris buffer at pH 7.4 at 35°C. Below 2.2 mM added PA, the observed PA based on the concentration determined from the PA $-CH_2$ signal follows a linear relationship with a slope of 0.41. Above 2.2 mM, the observed PA remains constant at 0.91 mM. Both MbCO and MbCN exhibit a similar non-specific PA interaction profile. The NMR visible PA fraction suggests a solubility that exceeds the corresponding PA solubility in Tris buffer.

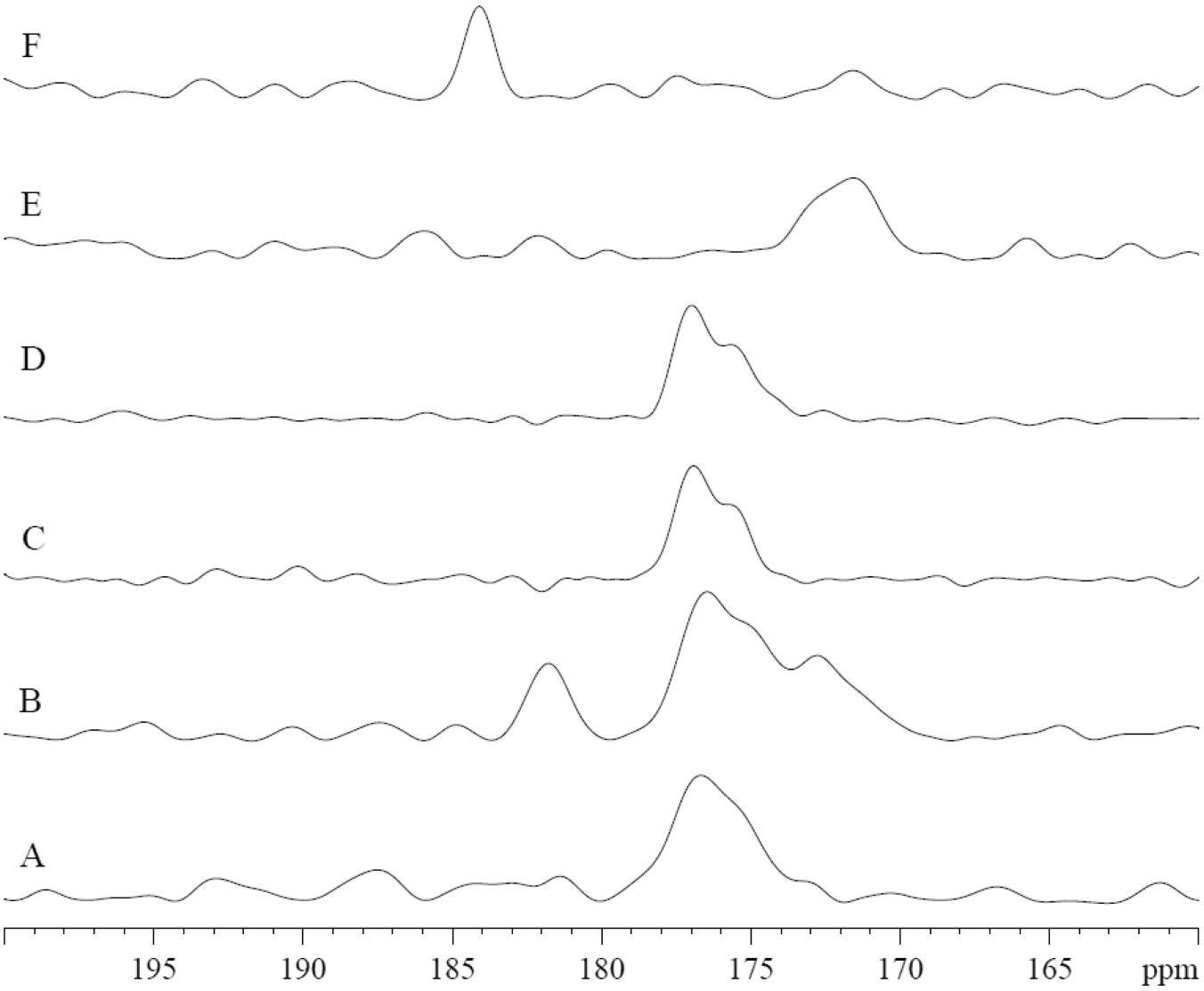

Figure 8.

$^{13}C_1$ PA in MbCO, deoxy Mb, and Tris exhibit contrasting spectra: A) 0.8mM MbCO in 30mM Tris buffer at pH 7.4 at 35°C B) 0.8 mM MbCO with 0.8 mM PA. PA peaks appear at 172 and 182 ppm, fig 8A–8B C) 0.8mM deoxy Mb D) 0.8mM deoxy Mb with 0.8 mM PA E) 3.2 mM PA in Tris buffer, pH 7.4. $^{13}C_1$ PA appears at 172 ppm. F) 3.2 mM PA in Tris buffer, pH 9.5. $^{13}C_1$ PA appears at 184 ppm.

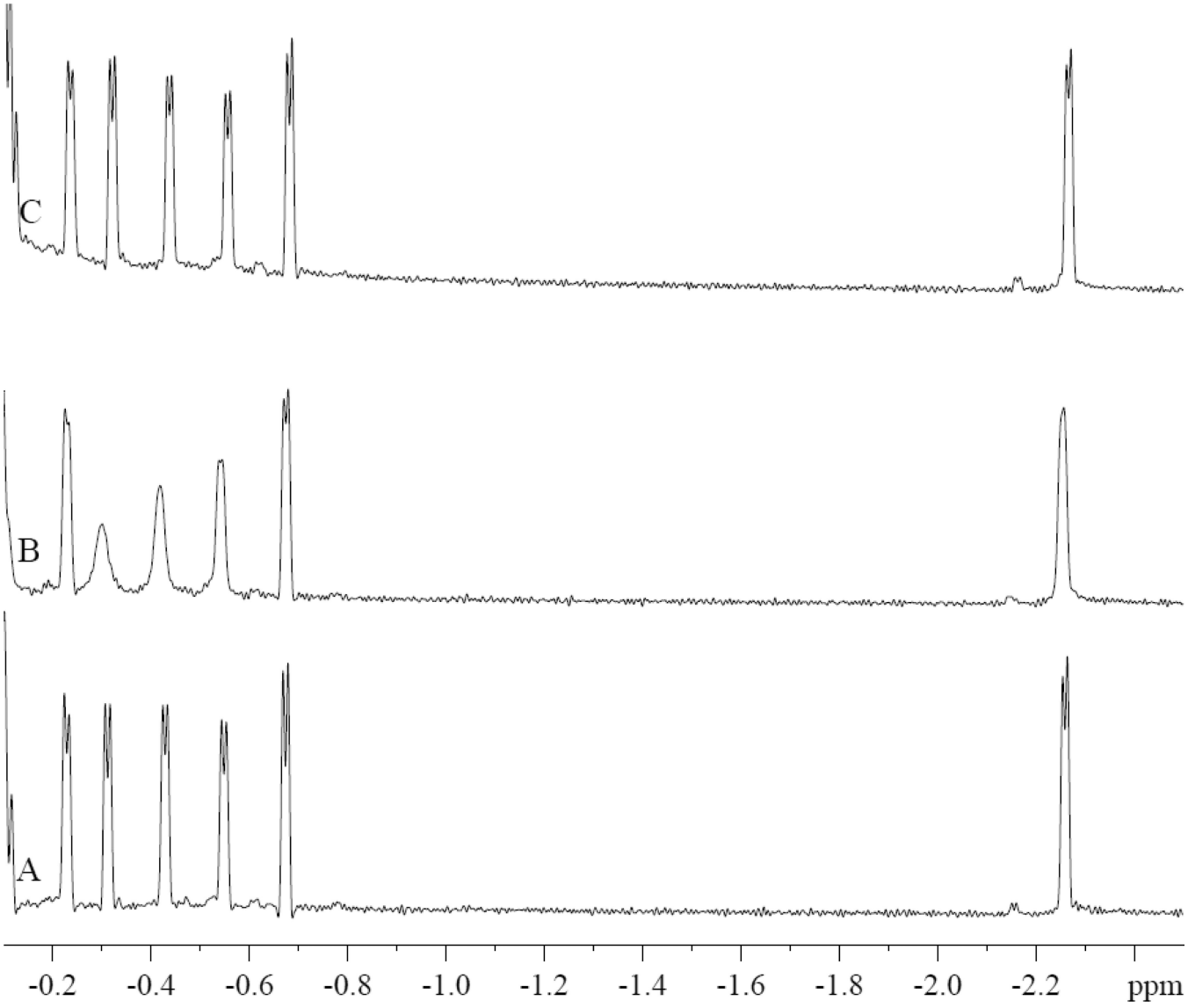

Figure 9.

Bovine serum albumin (BSA) and PA bound Mb. ^{1}H NMR spectra from A) 0.8 mM MbCN B) MbCN:PA 1:1 C) MbCN:PA:BSA 1:1:1. PA binding to Mb reduces selectively the intensity of peaks u4 and u5. Upon addition of BSA, these peaks restore to their respective control level.

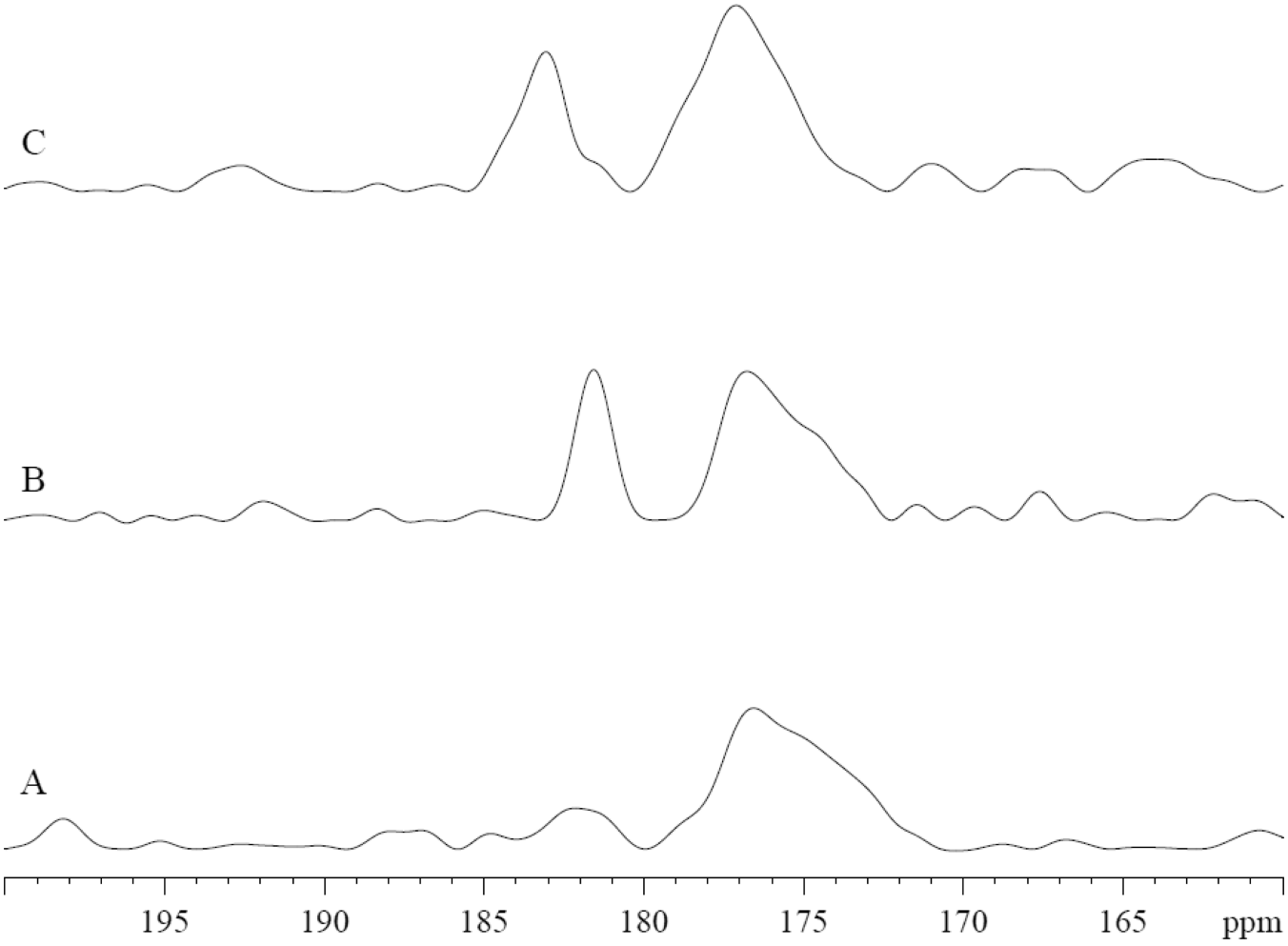

Figure 10.

Bovine serum albumin (BSA) and $^{13}C_1$ PA bound Mb. ^{13}C NMR spectra from A) 0.8 mM MbCN B) MbCN: $^{13}C_1$ PA 1:1 C) MbCN: $^{13}C_1$ PA:BSA 1:1:1. PA binding to Mb introduces a signal at 182 ppm. Upon addition of BSA, the signal shifts to 184 ppm. $^{13}C_1$ PA in BSA also shows a peak at 184 ppm (data not shown).

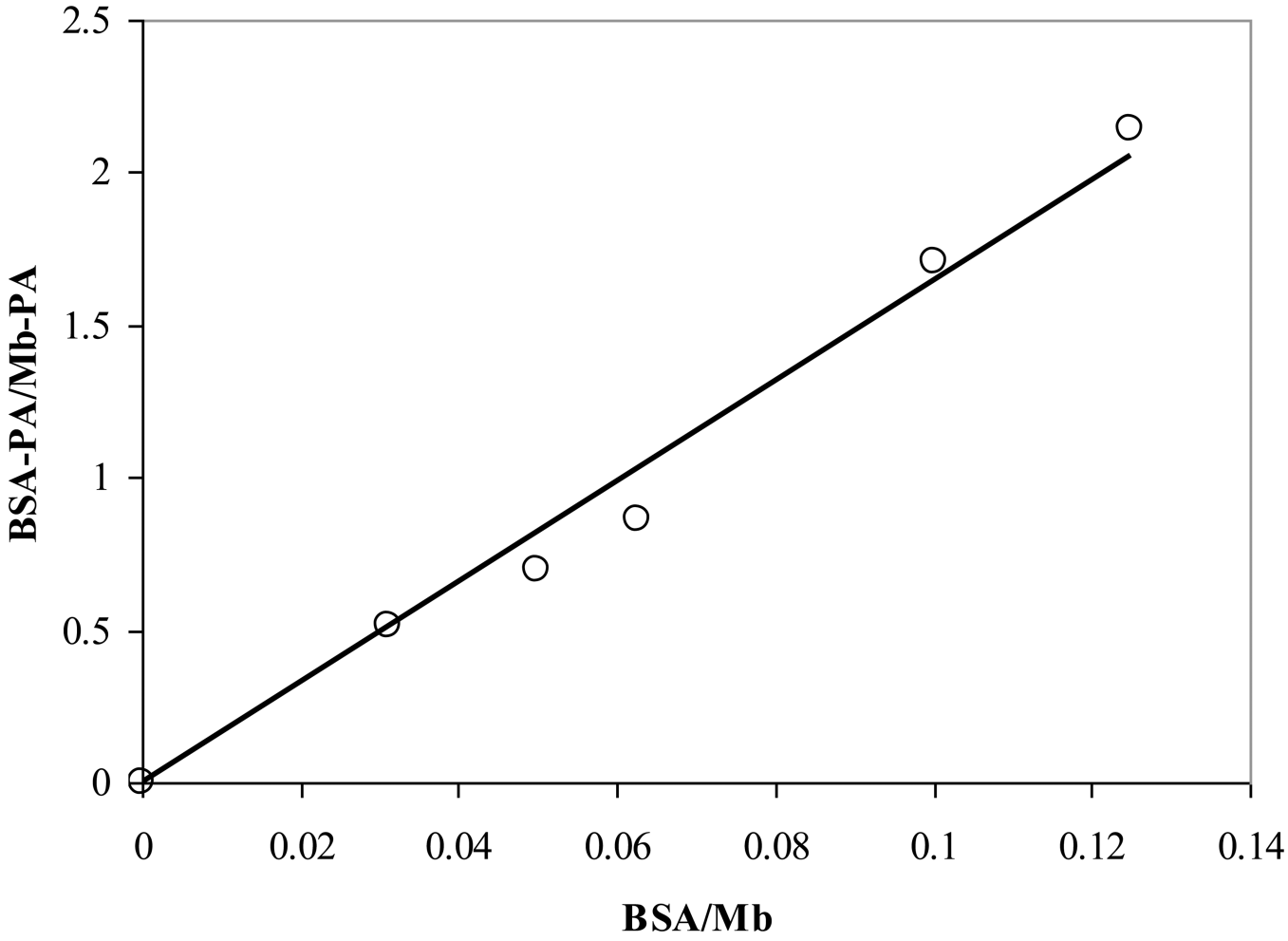

Figure 11.
Adding BSA to a 1:1 PA:Mb solution reveals a partition coefficient of 16 for the Mb vs. BSA PA affinity.

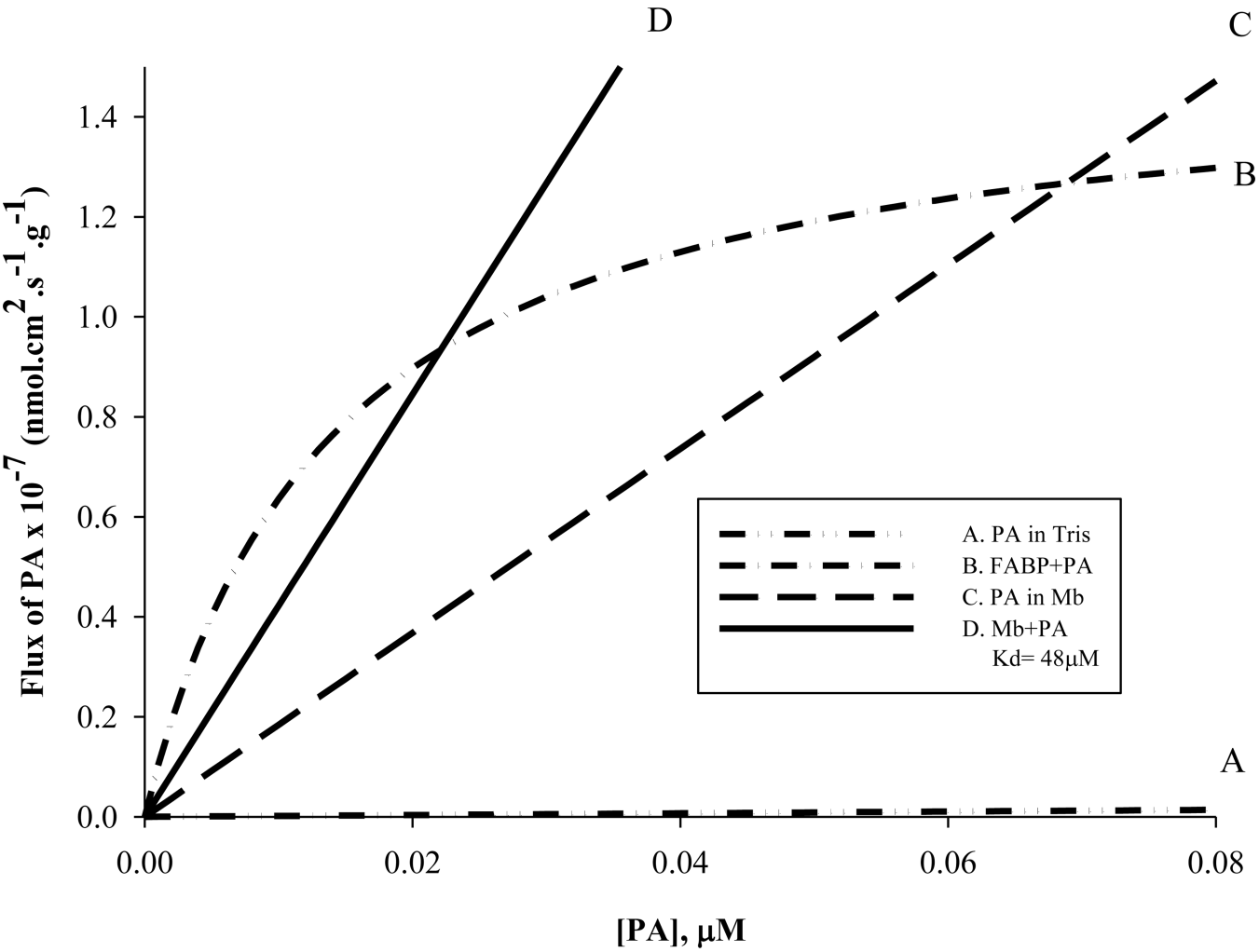

Figure 12.

Model of palmitate flux at low palmitate concentration: A) PA in Tris (0.8% solubility) B) FABP facilitated transport of fatty acid (50μM FABP, Kd=14nM) C) PA in the presence of Mb (41% solubility) D) Mb facilitated transport of PA (Mb=0.26mM, Kd=48μM). PA flux in the presence of Mb exceeds FABP facilitated PA flux above 0.07μM PA. Mb mediated transport of PA exceeds FABP-PA flux at PA concentration above 0.02 μM PA. The Vmax values per g tissue for FABP= 1.5×10^{-7} nmolcm^{2}s^{-1}g^{-1} for Mb=2.0×10^{-4} nmolcm^{2}s^{-1}g^{-1}. The corresponding 1/2 Vmax for FABP= 7.5×10^{-8} nmolcm^{2}s^{-1}g^{-1} and for Mb =1.0×10^{-4} nmolcm^{2}s1 −1 g .

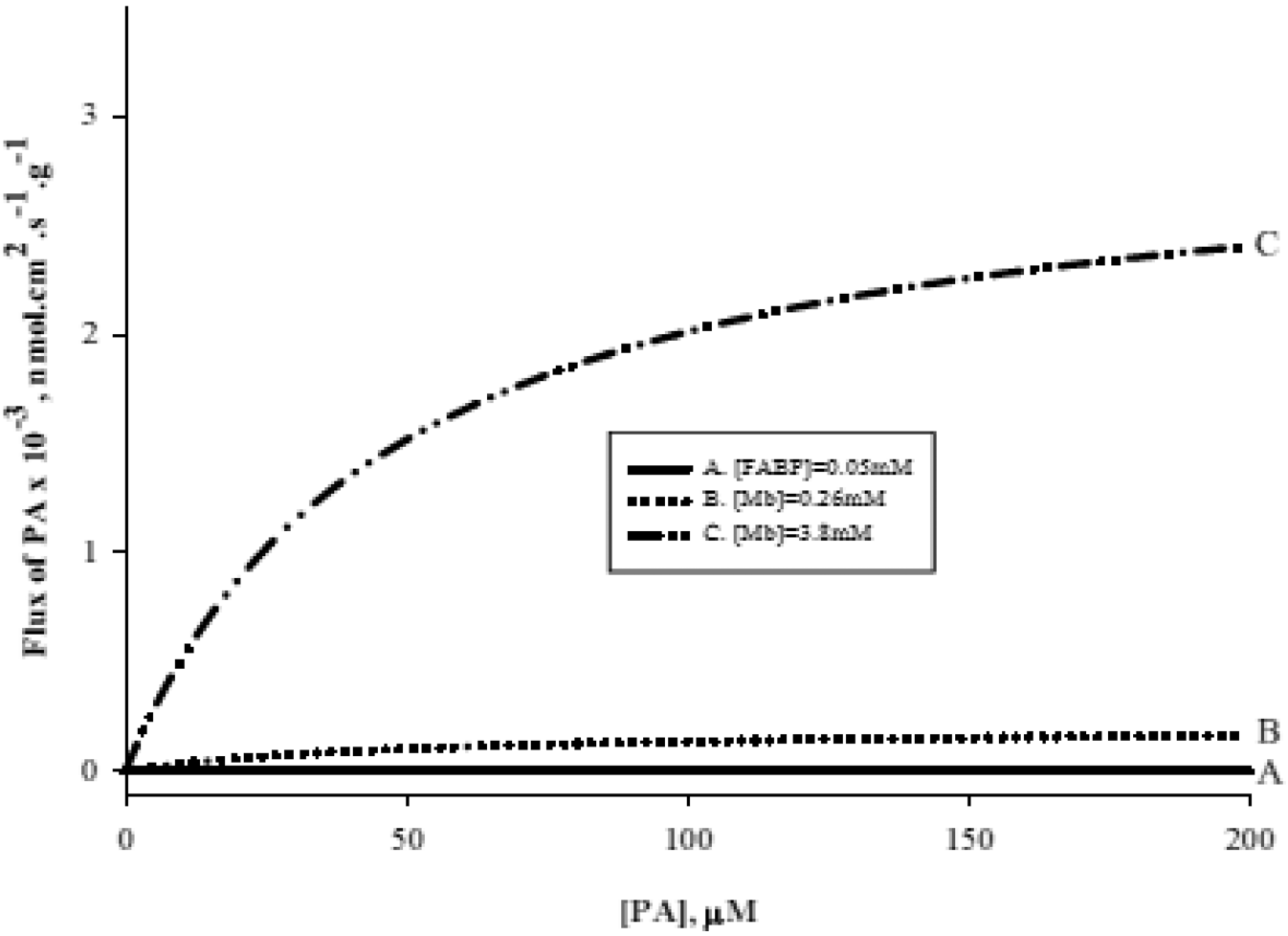

Figure 13.

Model of fatty acid flux at high palmitate concentration: A) FABP facilitated transport of fatty acid (50μM FABP, Kd=14nM) B) Mb facilitated transport of PA (Mb=0.26mM, Kd=48μM) C) Mb facilitated transport of PA (Mb=3.8 mM, Kd=48μM). The Vmax values per g tissue for Mb facilitated fatty acid transport in rat heart =2.0×10^{-4} $nmolcm^2s^{-1}g^{-1}$ and in seal muscle = 30×10^{-4} $nmolcm^2s^{-1}g^{-1}$

Table 1

Palmitate Solubility in Different Solutions

Solution	Solubility (M)	Solubility (g/100g solvent)	Reference
0.8 mM MbCN in Tris, pH 7.4 35°C	0.90×10^{3}	2.50×10^{-2}	This work
0.8 mM MbCO in Tris, pH 7.4 35°C	0.90×10^{-3}	2.50×10^{-2}	This work
*0.8 mM deoxy Mb in Tris, pH 7.4 35°C	Not detectable	Not detectable	This work
Tris buffer pH 7.4 35 °C	3.16×10^{-6}	8.79×10^{-5}	[67]
0.2 mM MbCN in Tris, pH 7.4 35°C	0.13×10^{-3}	3.62×10^{-3}	[67]
0.2 mM Lysozyme in Tris, pH 7.4 35°C	0	0	[67]
99.4% of Ethanol at 30°C	0.93	23.9	[55]
Acetone at 30°C	0.61	15.6	[55]
Benzene at 30°C	1.35	34.8	[55]
Glacial acetic acid at 30°C	0.31	8.11	[55]
66 mM Phosphate buffer, pH 7.4 at 37°C	$<10^{-10}$	$<2.78 \times 10^{-9}$	[70]
Water 20°C	6.00×10^{-7}	1.53×10^{-5}	[54]
Water, pH 5.7, 25°C	2.68×10^{-6}	6.87×10^{-5}	[61]
Water 30°C	3.2×10^{-5}	8.3×10^{-4}	[55]

*No detectable NMR signal of palmitate.

Table 2

Fatty acid flux model parameters

Parameter		Value	Reference
Concentration, rat heart (μM)	FABP (C_{FABP})	50	[68]
	Myoglobin (C_{Mb})	260	[48]
Dissociation Constant (μM)	KMb	48.3	This Work
	K_{FABP}	14.0×10^{-3}	[21,60].
Diffusion Constant (D, cm^2s^{-1})	Fatty acid (D_{FA})*	4.6×10^{-6}	[68]
	FABP (C_{FABP})	3.05×10^{-9}	[45]
	Myoglobin (C_{Mb})	7.85×10^{-7}	[43]
Equipoise [PA] at Flux A= Flux B (μM)	Mb & FABP	0.02	This Work
	PA in Mb & FABP	0.07	This Work
Maximum Facilitated Fatty Acid Flux ($nmolcm^2s^{-1}g^{-1}$)	Mb in Rat Heart	2.0×10^{-4}	This Work
	Mb in Seal Muscle	30.0×10^{-4}	This Work
	FABP	1.5×10^{-7}	This Work
PA Solubility (M)**	Tris	3.16×10^{-6}	[67]
	MbCN	0.97×10^{-3}	This Work
	MbCO	0.97×10^{-3}	This Work
	Deoxy Mb	Not Detectable	This Work

*The reported fatty diffusion coefficient, D_{FA}, varies widely. The fatty flux model has used the fastest reported diffusion coefficient of 4.6×10^{-6} cm^2/s to set an upper bound contribution for free FA flux.

**Solubility estimated from the observed ^1H NMR visible $–CH_2$ signal of palmitate in a 0.4 mM Mb solution.